Ligand Effects on Phase Separation of Multivalent Macromolecules

Kiersten M. Ruff [a,b,1,2], Furqan Dar [b,c,1], and Rohit V. Pappu [a,b,2]

[a] Department of Biomedical Engineering, [b] Department of Physics, [c] Center for Science & Engineering of Living Systems (CSELS), Washington University in St. Louis, St. Louis MO 63130

[1] K.M.R. and F.D. contributed equally to this work

[2] To whom correspondence may be addressed: kiersten.ruff@wustl.edu; pappu@wustl.edu

Abstract

Biomolecular condensates are thought to form via phase transitions of multivalent macromolecules. Components of condensates have been classified as *scaffolds* and *clients*. In this classification, scaffolds drive condensate formation whereas clients partition into condensates. However, non-scaffold molecules can be ligands that modulate the phase behavior of scaffolds via preferential binding across phase boundaries. Here, we present computational results that explain how preferential binding of ligands to scaffold molecules in different phases can impact phase separation and the compositions of dense phases. We show that phase separation is destabilized by monovalent ligands. In contrast, multivalent ligands, depending on their mode of binding, can stabilize phase separation by serving as crosslinkers that network scaffold molecules. We also find that concentrations of scaffolds within dense phases are generally diluted by ligands. This arises because ligands destabilize condensates by preferentially binding to scaffolds in the dilute phase or because ligands have to be accommodated within dense phases when they bind preferentially to scaffolds in the dense phase. Importantly, we show that partition coefficients, which are routinely used for compositional profiling of condensates, say nothing about the regulatory impact of ligands on the phase behavior of scaffolds. Therefore, instead of measuring partition coefficients it becomes imperative to measure how ligands impact threshold concentrations of scaffolds. These measurements, performed as a function of ligand concentration, will help with understanding the regulation of condensates and enable the design of molecules that impact condensate formation or dissolution.

Significance

Biomolecular condensates serve as organizers of biochemical reactions within cells. Growing evidence implicates multivalent biomacromolecules as drivers of condensate formation. Molecules that drive condensate formation are referred to as scaffolds. Here, we show that non-scaffold molecules are more than just clients of condensates. Instead, they can be ligands that stabilize or destabilize condensates by binding preferentially to scaffolds within the condensate or the dilute phase. Our findings suggest that ligands that modulate scaffold phase behavior can regulate condensates in cells. We also show that partition coefficients are uninformative for describing how non-scaffold molecules impact condensate formation or dissolution. We build on this to highlight the types of measurements that are imperative for understanding the formation / dissolution of condensates.

\body

Membraneless biomolecular condensates concentrate biomolecules in cells and organize biochemical reactions (1, 2). There is growing evidence that condensates form via spontaneous or driven phase transitions (2, 3) such as percolation (4) aided by liquid-liquid (5), liquid-liquid crystalline (6), or liquid-solid phase separation (7-9). In a binary mixture comprising macromolecules dissolved in an aqueous solvent, liquid-liquid phase separation gives rise to two coexisting phases – a dilute liquid phase that is deficient in macromolecules and a dense liquid phase that is enriched in macromolecules. The concentration threshold for phase separation, known as the saturation concentration, is set by the three-way interplay of inter-macromolecule, macromolecule-solvent, and solvent-solvent interactions (10, 11).

Cellular condensates include more than one type of macromolecule. Indeed, compositional profiling of condensates has shown that many of these bodies encompass hundreds of distinct types of protein and RNA molecules (1, 12-14). Banani et al., introduced the nomenclature of *scaffolds* and *clients* to distinguish different macromolecular constituents of multicomponent condensates (1, 15). In this parlance, scaffolds are macromolecules that are essential for condensate formation. Scaffolds often encompass multiple interaction domains / motifs and this is a defining hallmark of macromolecules that drive phase separation (15, 16).

The working hypothesis is that only a small fraction of the macromolecules that make up condensates are scaffolds. This hypothesis is supported by *in vitro* reconstitutions of facsimiles of condensates often using no more than two or three distinct types of macromolecules (1, 15). Banani et al., designated non-scaffold molecules as clients because they are not required for condensate formation. Further, a molecule is designated as a client based on experimental measurements of a partition coefficient (*PC*). This quantity is defined as the ratio of the concentration of the molecule in the dense versus the dilute phase. A molecule with a *PC* that is greater than one is classified as a client (1, 15). Empirically, scaffolds and clients can be distinguished by the number (valence) of interaction domains / motifs and the interaction strengths among domains. Scaffolds have a higher valence and clients have a lower valence of the motifs that drive condensate formation.

Although scaffolds are the drivers of condensate formation, the solution conditions and concentration regimes in which formation and dissolution of condensates occurs can be regulated by controlling the concentrations of non-scaffold molecules (17, 18) or via post-translational modifications to scaffolds (16, 19). An example of regulation by non-scaffold molecules comes from recent work on stress granules showing the different effects of Caprin-1 and USP-10 on the stability and integrity of stress granules (12, 20, 21). This example highlights the need for additional focus on and understanding of regulation by non-scaffold molecules, as dysregulation of condensate formation and dissolution can lead to disease (8, 9).

It is worth noting that the definition of a client says nothing about whether or how a non-scaffold molecule regulates scaffold phase behavior. Therefore, building on theories of binding and linkage, we refer to non-scaffold molecules that modulate scaffold phase behavior as ligands. We further stipulate that ligands do not undergo phase separation on their own and are not required for the phase separation of scaffolds. To understand the mechanisms that underlie the regulation of scaffold phase behavior by ligands, we coopt the *polyphasic linkage* formalism of Wyman and Gill (22). This formalism lays out how ligands, depending on their concentration, can act as modulators of scaffold phase behavior. The existence of a phase boundary sets up the possibility

of preferential binding to scaffolds in one phase over the other; a ligand can have a higher affinity for the scaffold in the dense phase over the dilute phase or vice versa.

For a ligand to bind preferentially to a scaffold in one of the two phases, there has to be an asymmetry in binding to the scaffold in the dilute versus the dense phase. Asymmetry in binding arises because of differences in scaffold concentration and accessibility of scaffold sites across the phase boundary. For example, scaffold sites that drive phase separation can become inaccessible to ligands in the dense phase. Additionally, the higher concentration of scaffolds in the dense phase compared to the dilute phase can allow for a multivalent ligand to crosslink multiple scaffolds which can increase the effective affinity of the ligand with the scaffold in the dense phase. The scaffold can also undergo conformational changes across the phase boundary, and this can modulate the accessibility of scaffold sites.

To illustrate the concepts of polyphasic linkage, we shall consider an aqueous solution with a single type of scaffold that separates into two distinct phases. We denote the dilute phase as *A* and the coexisting dense phase as *B*. The binodal or coexistence curve delineates the two-phase regime (**Fig. 1A**). For a given set of solution conditions quantified in terms of an effective interaction strength, the left arm of the binodal denotes the saturation concentration in the dilute phase, c_A and the right arm of the binodal corresponds to the concentration of the scaffold in phase *B*, c_B. For fixed interaction strengths, c_A and c_B remain constant but the relative volumes of the two phases vary as the total concentration of the scaffold changes. For concentrations below c_A and above c_B, the system is in the single-phase regime.

The polyphasic linkage formalism describes how ligand binding modulates c_A of the scaffold for fixed solution conditions. The value of c_A in the presence of the ligand, designated as c_A^L is set by equalization of the chemical potential of the scaffold across the phase boundary. This yields the expression $c_A^L = c_A\left(\frac{P_A}{P_B}\right)$ (22). Here, P_A and P_B are the binding polynomials that quantify binding of the ligand to the scaffold in phases *A* and *B*, respectively. It follows that if P_A is greater than P_B, then the ligand preferentially binds to the scaffold in phase *A*. Preferential binding of the ligand to the scaffold in the *A* phase will lead to an increase in c_A^L compared to c_A, thus weakening the driving forces for phase separation of the scaffold (**Fig. 1A**). Conversely, if P_B is greater than P_A, then the ligand preferentially binds the scaffold in the dense phase *B*. Accordingly, c_A^L decreases when compared to c_A. In this scenario, preferential binding of the ligand to the scaffold in the dense phase will enhance the driving forces for phase separation as evidenced by lowering of the threshold concentration to be crossed in order for the system to undergo phase separation (**Fig. 1B**). In the absence of preferential binding, the ligand binds equivalently to the scaffold in both phases, implying that $c_A^L = c_A$ and ligand binding does not modulate the phase equilibrium.

Recent studies suggest that scaffolds, which are multivalent macromolecules, can be thought of as biological instantiations of associative polymers (23, 24) and modeled using the so-called *stickers*-and-*spacers* framework (4, 25-29). Accordingly, the valence (number) of stickers, the sticker interaction strengths, and the solvation properties of spacers contribute as determinants of the phase behavior of multivalent protein and RNA molecules (30-32). Here, we use a combination of coarse-grained simulations and theory to answer the following questions: (1) How doe the valence of sticker and / or spacer binding motifs in ligands and the affinities for

complementary sites on scaffolds influence the overall phase diagrams of scaffolds? (2) Do partition coefficients provide insights regarding the preferential binding and modulatory effects of ligands? (3) And what quantities should be measured in order to understand the effects of ligands on the phase behavior of scaffolds? Answers to these questions are directly relevant to an improved understanding of how ligands contribute to the modulation and regulation of the phase behavior of scaffolds. They are also directly relevant to the design of therapeutics that alter the phase behavior of scaffolds (33, 34).

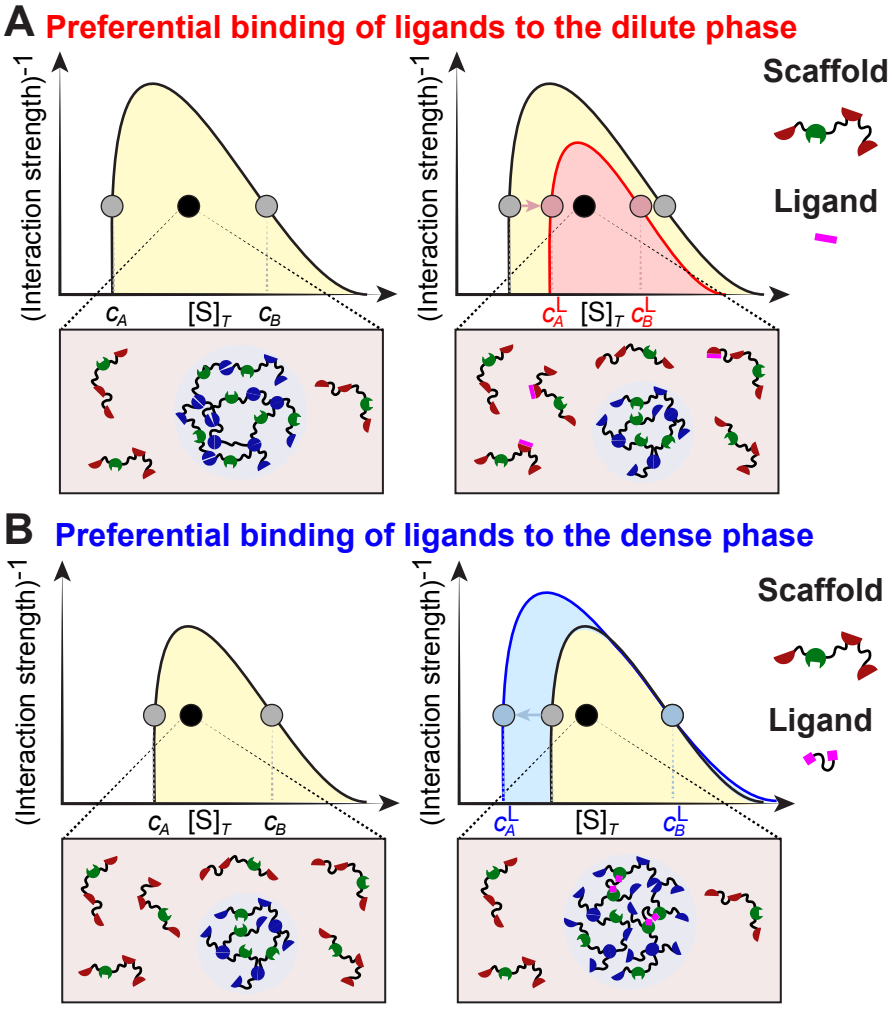

Figure 1: The phase behavior of scaffolds can be modulated by ligands. In this schematic, we assume that the scaffolds undergo phase separation and form two distinct phases: the dilute phase (red), *A*, and the dense phase (blue), *B*. In panels **A** and **B**, the yellow region, bounded by the coexistence curve (the binodal) delineates the two-phase regime of the scaffold. The phase diagram is drawn in the two-parameter space of total scaffold concentration, $[S]_T$, and effective interaction strength among scaffold molecules. For a given value of the interaction strength along the ordinate, the left arm of the binodal represents the saturation concentration, c_A, and the right arm of the binodal denotes the concentration of the scaffold in the dense phase, c_B (grey circles). The polyphasic linkage formalism describes how c_A changes by way of preferential binding of the ligand across the phase boundary and this is denoted as c_A^L. (**A**) $c_A^L > c_A$ if the ligand preferentially

binds to the scaffold in the dilute phase; (**B**) $c_A^L < c_A$ if the ligand preferentially binds to the scaffold in the dense phase.

Results

Our goal is to uncover general rules that summarize the effects of different types of ligands on scaffold phase behavior. Accordingly, we deployed coarse-grained simulations to understand how different types of ligands modulate the phase behavior of model linear multivalent macromolecules. While the polyphasic linkage formalism can be used to uncover the impact of ligand binding on scaffold concentrations in the dense phase, to do so is non-trivial and requires system-specific treatments (22). Accordingly, the original formulation of polyphasic linkage makes the implicit assumption that $c_B^L = c_B$. Here, we address this and other issues using Monte Carlo simulations using the lattice simulation engine LASSI (35). Details are described in the *SI Appendix*. The simulations allow us to probe the effects of ligand binding on the full phase diagram of the scaffold. This includes the low concentration arm, the critical point, and the high concentration arm. Linear multivalent macromolecules are represented by *stickers* and *spacers*. Here, spacers can be implicit, in that they do not take up volume, or they can be explicit, in that they occupy volume on the lattice.

Model used in LASSI simulations: In our model system, the scaffold molecule contains five sticker sites and two explicit spacer sites (**Fig. 2A**). We consider five different ligand types (**Fig. 2C**): (i) a monovalent ligand that interacts exclusively with scaffold stickers; (ii) a monovalent ligand that interacts exclusively with scaffold spacers; (iii) a divalent ligand that interacts exclusively with scaffold stickers; (iv) a divalent ligand that interacts exclusively with scaffold spacers; and (v) a divalent ligand that interacts with scaffold stickers and spacers. The only attractive interactions in the system are between pairs of sticker sites on scaffolds and between scaffold sticker or spacer sites and the ligand. The details of the latter will depend on the type of ligand being considered. We consider three energy scales for the ligand-scaffold interaction: E_1, the ligand-scaffold interaction is half that of the scaffold-scaffold interaction, E_2, the ligand-scaffold interaction is equal to the scaffold-scaffold interaction, and E_3, the ligand-scaffold interaction is double that of the scaffold-scaffold interaction. For each case, we performed five independent simulations.

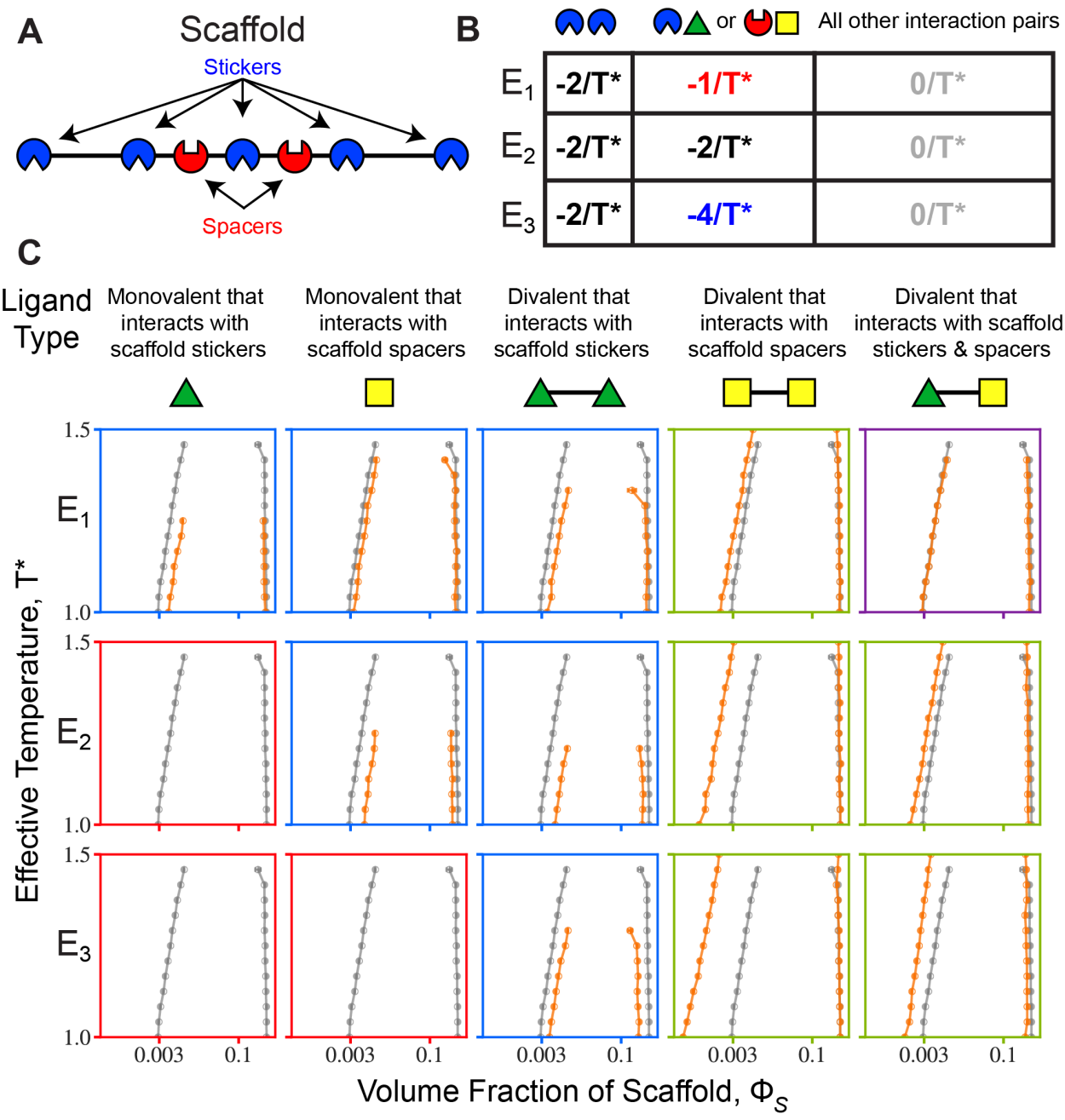

Figure 2: Effect of ligand types on scaffold phase behavior. (**A**) Schematic of the scaffold molecule used in coarse-grained simulations. The molecule has five sticker sites and two explicit spacer sites (the remaining two spacer sites are implicit). (**B**) Three energy scales were examined to assess how the different ligands modulate scaffold phase separation. (**C**) Binodals of the scaffold in the absence of ligand (grey) and in the presence of the given ligand (orange) for the three different energy scales, E_1, E_2, and E_3. The bounding boxes for each case are color coded to summarize the effect of each ligand on scaffold phase separation: red – ligand binding abolishes phase separation, blue – ligand binding destabilizes phase separation, purple – ligand binding does not change phase separation, and green – ligand binding promotes phase separation.

Quantifying the effects of different types of ligands on full phase diagrams: **Fig. 2C** shows the binodals for the scaffold without ligand and the impact of ligand binding. In each case, we show results for a ratio of 0.23 for the ligand to scaffold sites (or a ratio of 0.8 divalent ligands to scaffold molecules). For this ratio, we observe four categories of ligand-modulated phase behaviors of scaffolds: (1) Ligand binding abolishes scaffold phase separation (phase diagrams with red bounding boxes in **Fig. 2C**), (2) ligand binding destabilizes scaffold phase separation (phase diagrams with blue bounding boxes in **Fig. 2C**), (3) ligand binding does not impact phase separation (phase diagrams with purple bounding boxes in **Fig. 2C**), and (4) ligand binding promotes phase separation (phase diagrams with green bounding boxes in **Fig. 2C**). Results for three additional ligand-to-scaffold ratios are shown in the *SI Appendix* (**Fig. S1-S3**), and the results are qualitatively similar to those shown in **Fig. 2C**.

Monovalent ligands destabilize or abolish scaffold phase separation, and this is true irrespective of whether they interact with sticker or spacer sites (columns 1 and 2 of **Fig. 2C**). Monovalent ligands that interact directly with sticker sites reduce the effective valence of stickers, whereas monovalent ligands that interact directly with spacer sites reduce the cooperativity of phase transitions (31). The reduction in cooperativity refers to weakening the growth of the network by increasing the effective excluded volume of spacers, thereby inhibiting sticker-sticker interactions, as discussed by Harmon et al. (31).

Divalent ligands that interact directly with sticker sites on scaffolds destabilize phase separation by competing with the sticker-sticker interactions that drive phase separation (column 3 of **Fig. 2C**). In contrast, phase separation is stabilized by divalent ligands that interact with scaffold spacer sites (column 4 of **Fig. 2C**). Here, the divalent ligand acts as a crosslinker that enables increased networking of the multivalent macromolecules. Increased networking of multivalent scaffolds by multivalent has been demonstrated for including patchy colloidal particles (36), which are facsimiles of folded domains with stickers on their surfaces (4). Divalent ligands that bind both sticker and spacer sites of scaffolds show an intermediate effect compared to the other two divalent ligands. They can promote phase separation at higher interaction strengths; however, this effect is weaker when compared to that of divalent ligands that bind only to spacer sites (column 5 of **Fig. 2C**).

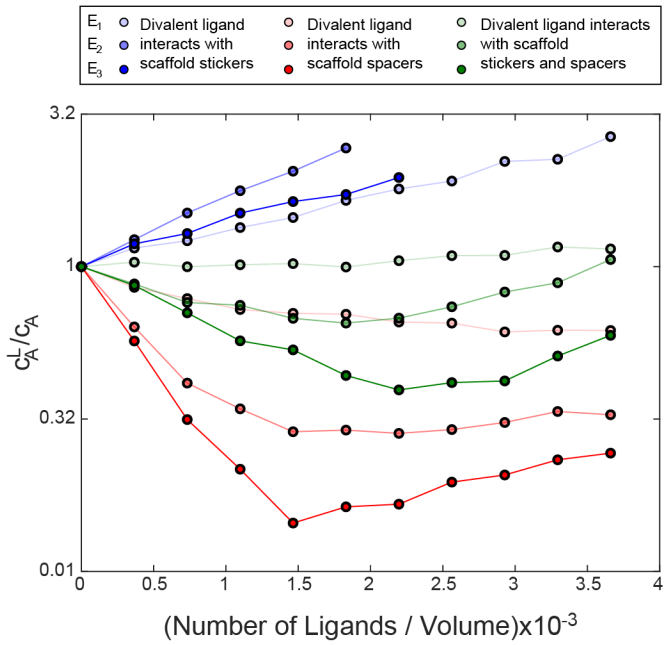

Figure 3: Changes to $\left(\frac{c_A^L}{c_A}\right)$ as a function of divalent ligand concentration at T*≈1.08 for different energy scales. As each color becomes darker the interaction strength between the scaffold and the ligand is increased. Data are plotted only if the system undergoes phase separation, i.e., the width of the two-phase regime satisfies the criterion $\left(c_B^L - c_A^L\right) > 0.15$.

Quantifying the effects of different types of ligands on the change to c_A: Experimental characterizations of full binodals are challenging, and accordingly, these measurements have been performed only for a small number of scaffold molecules (37-40). In contrast, it is easier to measure changes in saturation concentrations in the absence (29) and the presence of ligands (21, 33). To set up expectations regarding how saturation concentrations change, we analyze how the ratio $\left(\frac{c_A^L}{c_A}\right)$ changes as a function of divalent ligand concentration (**Fig. 3**). This analysis was performed at a constant simulation temperature across all systems. At a given ligand concentration, the greater the deviation between c_A^L and c_A, the greater the asymmetry in the preferential binding of the ligand to the scaffold in either the dense or dilute phase.

For all ligand concentrations and interaction strengths tested, the divalent ligand that interacts with scaffold stickers causes an increase in c_A^L. At the highest tested ligand concentrations and interaction strengths, phase separation is abolished. In contrast, the divalent ligand that interacts with scaffold spacers decreases c_A^L for all ligand concentrations and interaction strengths tested, thus promoting scaffold phase separation. At high ligand concentrations, we observe a reversal in the trend of c_A^L decreasing with increasing ligand concentrations. A similar effect has been reported recently in experiments that characterized the phase behavior of poly-SH_3-poly-PRM system in the presence of increased concentrations of the ligand heparin (41). For this system, the turnover behavior was hypothesized to be due to electrostatic repulsions of heparin at high

concentrations. Charge effects were not included in our model and, therefore, they cannot be the source of the observed turnover in our simulations. Instead, the simplest explanation is that at high ligand concentrations, there is a competition between the crosslinking effects of divalent ligands and the binding of excess ligands to spacer sites, such that the crosslinking ability is weakened.

The effects of the bipartite divalent ligand that interacts with sticker and spacer sites on scaffolds will depend on the interaction strengths and ligand concentration. At the lowest interaction strength, E_1, the ligand causes minimal changes to c_A^L when compared to c_A. However, there is a modest destabilization of scaffold phase separation at the highest ligand concentrations. At higher interaction strengths and low ligand concentrations, the ligand promotes phase separation, but to a weaker extent than the divalent ligand that interacts purely with spacer sites on scaffolds. Similar to the divalent ligand that interacts with spacer sites on scaffolds, the bipartite divalent ligand also engenders a turnover behavior in the dependence of c_A^L on ligand concentration. It appears that this turnover behavior is a general feature of ligands that promote phase separation by preferentially binding to scaffolds in the dense phase. The ligand concentration at which turnover is observed will provide an estimate of the ligand-dependent concentration of scaffold sites i.e., the concentration of scaffold sites within the dense phase where ligands switch from crosslinking or networking to binding primarily to the same scaffold.

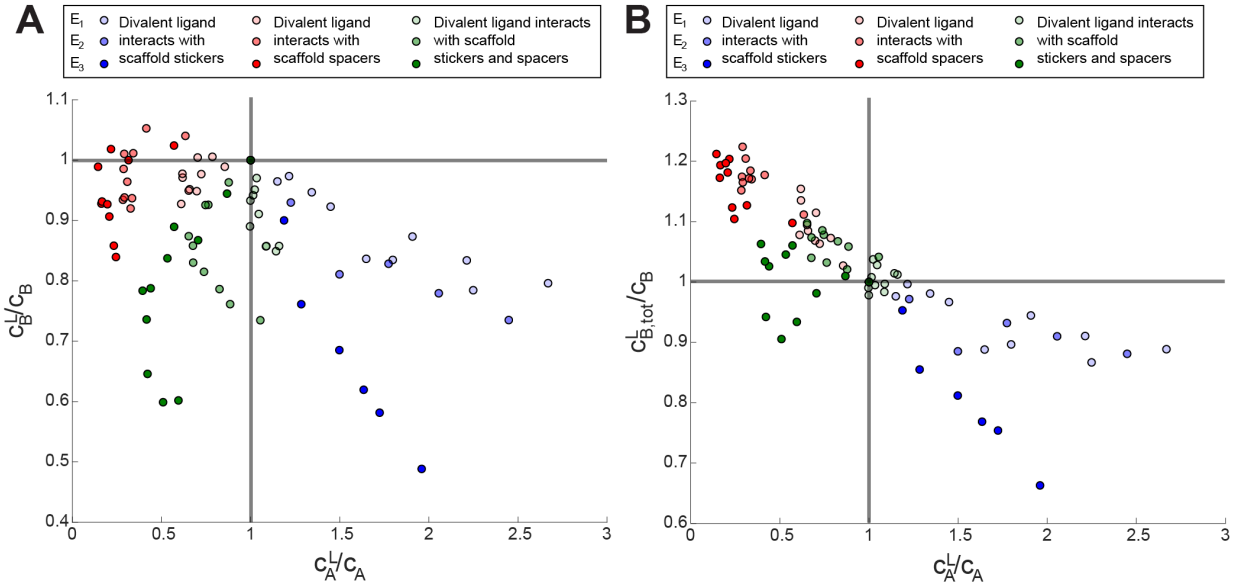

Fig. 4: Change in dense phase versus dilute phase concentrations as a function of ligand type, interaction strength, and ligand concentration at T*≈1.08. (A) Change in the scaffold dense phase concentration plotted against the change in the scaffold dilute phase concentration. (B) Change in the total concentration of scaffolds and ligands ($c_{B,\mathrm{tot}}^L$) in the dense phase plotted against the ligand-modulated change in the dilute phase concentration of the scaffold. The darkening of the point color denotes an increase in interaction strength between the scaffold and the ligand. Points in the upper left quadrant indicate that the concentration in the dense phase has increased, whereas the concentration in the dilute phase has decreased in comparison to the scaffold only phase behavior. Points in the lower right quadrant indicate the dense phase concentration has decreased and the dilute phase concentration has increased in comparison to the scaffold only

phase behavior. The latter corresponds to a shrinking of the width of the two-phase regime. Data are plotted only if the system undergoes phase separation, i.e., the width of the two-phase regime satisfies the criterion $\left(c_B^L - c_A^L\right) > 0.15$.

Quantifying the impact of ligands on scaffold concentrations and the total concentration of molecules in the dense phase: **Fig. 4** shows the change in the scaffold and total dense phase concentrations in the presence of each of the divalent ligand types that were modeled using different energy scales compared to the behavior of the scaffold alone. The key observations are as follows: The scaffold concentration in the dense phase generally does not increase above the ligand-free case regardless of how ligand binding influences c_A (**Fig. 4A**, few points in the upper left quadrant). Ligands, irrespective of whether they enhance or weaken phase separation, will have a diluting effect on scaffolds within the dense phase and this effect increases with increasing ligand concentration (*SI Appendix* **Fig. S4**). The extent of dilution depends on the interaction mode, interaction strengths, and ligand concentration. Specifically, binding to sticker sites on scaffolds has a greater effect on reducing the scaffold concentration in the dense phase, and this effect is increased as the interaction strength between the scaffold and ligand is increased. The ligand-mediated dilution of scaffolds within the dense phase reflects the constraints of excluded volume whereby the scaffold has to accommodate the ligand within the condensate.

We next assessed the extent to which dilution of the scaffold concentration within condensates is compensated by an increase in ligand concentration. We quantified the total concentration of scaffolds *and* ligands in the dense phase for each of the different ligand types. The results, shown in **Fig. 4B**, may be summarized as follows: ligands that promote phase separation tend to increase the total dense phase concentration (upper left quadrant in **Fig. 4B**); ligands that do not alter the driving forces for phase separation tend to maintain the total dense phase concentration (light green points in **Fig. 4B**); and ligands that destabilize phase separation tend to decrease the total dense phase concentration (blue points in **Fig. 4B**).

Partition coefficients do not provide information regarding preferential binding effects of ligands: Can one determine if a ligand destabilizes or promotes phase separation by measuring the *PC* of a ligand? To answer this question, we calculated the *PCs* for all ligands shown in **Fig. 3**. **Fig. 5** shows that the calculated *PCs* are all greater than one, even for ligands that destabilize scaffold phase separation. Ghosh et al., (41) reported similar results in their experimental characterization of the poly-SH_3 : poly-PRM system. For our system, we find that *PC* values spanning from 10 to 100 can correspond to ligands that destabilize, do not change, or promote scaffold phase separation. The exact value for this range will be system dependent. The most important takeaway is that a *PC* being greater than some threshold value does not imply that the ligand preferentially binds to the scaffold in the dense phase. Accordingly, *PC*s do not tell us if a ligand binds preferentially to scaffolds across the phase boundary.

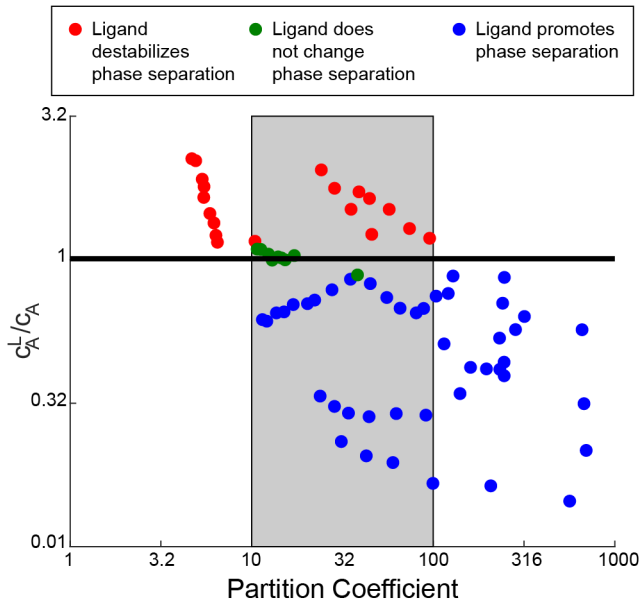

Fig. 5: Partition coefficients calculated for the divalent ligands. The changes in saturation concentration for all divalent ligands at T*≈**1.08** are plotted against the corresponding *PCs*. The grey box denotes a region of partition coefficients that is consistent with ligands that destabilize, do not change, or promote scaffold phase separation. Data are plotted only if the system undergoes phase separation, i.e., the width of the two-phase regime satisfies the criterion $\left(c_B^L - c_A^L\right) > 0.15$.

Linkage theory (22) *establishes that partition coefficients combine the contributions of preferential binding and local concentration effects*: The impact of ligand binding on saturation concentrations is written in terms of binding polynomials P_A and P_B that quantify the binding of the ligand in question to the scaffold in phases A and B, respectively. A binding polynomial is the partition function of the ligand plus scaffold system and is a sum over the activities of all states in the system involving the scaffold relative to the free scaffold (42). We shall assume we have a system where the ligand binding to the scaffold is described by a first order polynomial in both phases. The *SI Appendix* shows results for higher order binding polynomials. Ligand binding is described using:

$$\begin{aligned} \left[S_A\right] + \left[L\right] &\rightleftharpoons \left[S_A L\right] \\ \left[S_B\right] + \left[L\right] &\rightleftharpoons \left[S_B L\right] \end{aligned} \tag{1}$$

Here, $[L]$, $[S_A]$, $[S_B]$, $[S_AL]$ and $[S_BL]$ are respectively the concentrations of free ligand, free scaffold in phase A, free scaffold in phase B, bound scaffold in phase A, and bound scaffold in phase B. The binding polynomial in the dilute phase is given by:

$$P_A = \frac{\left[S_A\right] + \left[S_A L\right]}{\left[S_A\right]} = 1 + \beta_A \left[L\right]; \tag{2}$$

Here, β_A is the cumulative association constant. Likewise, the binding polynomial in the dense phase is $P_B = 1+\beta_B[L]$. Accordingly, it follows that: $c_A^L = c_A\left(\frac{P_A}{P_B}\right) = c_A\left(\frac{1+\beta_A[L]}{1+\beta_B[L]}\right)$. It should be noted that this equation may not be valid for high concentrations of free ligand because it ignores non-idealities due to interactions of ligands with themselves. Additionally, it assumes that c_B does not change upon addition of the ligand. Despite these assumptions, the polyphasic linkage formalism can be deployed to uncover a phenomenological understanding of why partition coefficients behave as shown in **Fig.5**. Accordingly, we assess how c_A^L and the *PC* change as a function of the ratio $\beta_A\beta_B^{-1}$ and free ligand concentration [*L*]. The system is defined by the following set of equations:

$$\begin{gathered}\beta_A = \frac{[S_AL]}{[S_A][L]},\ \beta_B = \frac{[S_BL]}{[S_B][L]},\\ [S_A]_{\text{tot}} = [S_A]+[S_AL],\ [S_B]_{\text{tot}} = [S_B]+[S_BL],\\ \text{and } [L]_{\text{tot}} = [L]+[S_AL]+[S_BL];\end{gathered} \tag{3}$$

Here, $[S_A]_{\text{tot}}$ and $[S_B]_{\text{tot}}$ are the total scaffold concentrations in phases *A* and *B*, respectively, that are calculated using the total system volume *V*. Likewise, $[L]_{\text{tot}}$ is the total ligand concentration in the system. The total scaffold concentration is given by:

$$[S]_{\text{tot}} = \frac{n_A+n_B}{V_A+V_B} = \frac{n_A+n_B}{V} = [S_A]_{\text{tot}}+[S_B]_{\text{tot}}; \tag{4}$$

Here, n_A, n_B are the numbers of scaffold molecules within and V_A, V_B are the volumes of phases *A* and *B*, respectively; *V* is the total volume of the system. Accordingly, the saturation concentration $c_A^L = \frac{n_A}{V_A}$ is related to $[S_A]_{\text{tot}}$ as follows:

$$\begin{gathered}[S_A]_{\text{tot}} = \left(\frac{n_A}{V}\right)\left(\frac{V_A}{V_A}\right) = c_A^L\left(\frac{V_A}{V}\right) = c_A^L\phi_A,\\ \text{and } [S_B]_{\text{tot}} = [S]_{\text{tot}} - [S_A]_{\text{tot}} = [S]_{\text{tot}} - c_A^L\phi_A;\end{gathered} \tag{5}$$

It follows that the system of equations shown in (3) becomes:

$$\begin{gathered}[S_A]_{\text{tot}} = c_A^L\phi_A = [S_A]+[S_AL],\\ [S_B]_{\text{tot}} = [S]_{\text{tot}} - c_A^L\phi_A = [S_B]+[S_BL],\\ [L] = [L]_{\text{tot}} - [S_AL]-[S_BL];\end{gathered} \tag{6}$$

The *PC* is defined as the concentration of the ligand in the dense phase (*B*) divided by the concentration of the ligand in the dilute phase (*A*). In both phases the ligand can be free or bound, and the partitioning of free ligand between the two phases is governed by the relative volumes of each phase. In the above equations, all concentrations, except c_A^L are computed with respect to the

total volume (V) of the system. However, for *PC*, the concentrations are computed with respect to the volumes of the individual phases. Therefore, it follows that:

$$PC = \left(\frac{\phi_A}{1-\phi_A}\right)\left(\frac{\left[S_B L\right]+\left(1-\phi_A\right)\left[L\right]}{\left[S_A L\right]+\phi_A\left[L\right]}\right); \quad (7)$$

The relation derived in equation (7) shows that the *PC* is dependent on the concentration of the ligand bound scaffold in each phase as well as the volume fractions of the two phases. We leverage the linkage relation shown in equations (3), (6), and (7) to quantify how c_A^L and *PC* change as a function of the ratio of association constants, $\beta_A\beta_B^{-1}$, and the free ligand concentration [L]. Specifically, we numerically solve equations (3) and (7) to determine c_A^L and *PC* for different values of β_A, β_B, c_A, c_B, $[S]_{tot}$ and [L] (**Fig. 6**). Results are shown for c_A = 1 μM, c_B = 19 μM, and $[S]_{tot}$ = 10 μM for three different ratios of $\beta_A\beta_B^{-1}$ (**Fig. 6**).

When the ligand binds preferentially to the scaffold in the dilute phase, $\beta_A\beta_B^{-1} > 1$ and c_A^L increases with ligand concentration; when the ligand binds preferentially to the scaffold in the dense phase $\beta_A\beta_B^{-1} < 1$ and c_A^L decreases with ligand concentration (**Fig. 6A**); finally, when the ligand binds equivalently to the scaffold in both phases $\beta_A\beta_B^{-1} = 1$ and $c_A^L = c_A$ for all ligand concentrations. For systems characterized by preferential binding of the ligand to scaffold sites in one phase over the other, the value of c_A^L begins to deviate from c_A as the free ligand concentration approaches the lowest dissociation constant i.e., when $\left[L\right] > \min\left(\beta_A^{-1}, \beta_B^{-1}\right)$. We also quantified how the *PC* varies with ligand concentration (**Fig. 6B**). Irrespective of the ratio $\beta_A\beta_B^{-1}$, we find that the *PC* is greater than one. This result is consistent with our simulation results and supports the finding that *PC* values do not yield direct information regarding the impact of a ligand on the phase behavior. This is because a *PC* is a convolution of the contributions from preferential binding and the higher concentration of scaffolds in the condensates. Furthermore, we find that the *PC* decreases with increasing free ligand concentration and is highest at low ligand concentrations where the ligand has limited modulatory effects on scaffold phase behavior. This result further highlights the lack of a direct relationship between preferential binding and *PC*.

Given that the free ligand concentration is not easily measurable, we plotted the change in saturation concentration and the *PC* values as a function of total ligand concentration (**Fig. 6 C-D**). The general takeaways are the same as when the quantities are plotted as a function of free ligand concentration. Quantifying the change in the saturation concentration as a function of free or total ligand concentration provides clear insights into how a ligand does or does not modulate scaffold phase behavior. In direct contrast, *PC*s do not provide insights regarding the effects of ligands on phase behavior and preferential binding.

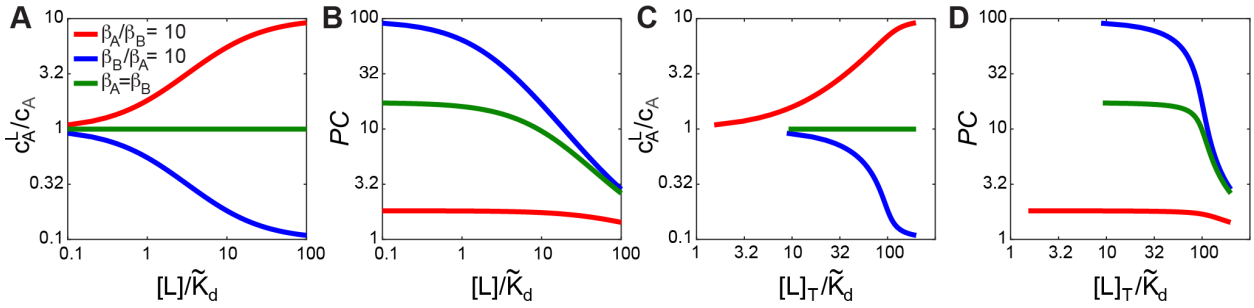

Fig. 6: Theory shows how saturation concentrations and partition coefficients change as a function of ligand concentration for ligands with different types of preferential interactions. Ligand concentrations ([L]) are normalized by $\tilde{K}_d = \min\left(\beta_A^{-1}, \beta_B^{-1}\right)$. Panels (A) and (C) plot the ratio $\left(\frac{c_A^L}{c_A}\right)$ against the normalized free ligand concentration (A) and normalized total ligand concentration (C). Panels (B) and (D) plot *PC* against the normalized free ligand concentration (B) and normalized total ligand concentration (D).

Discussion

Non-scaffold molecules are defined as molecules that do not undergo autonomous phase separation and are not required for the phase separation of scaffolds. These non-scaffold molecules are designated as being clients if their *PCs* are greater than one (1, 15). We propose that this designation needs generalization to include the effects of ligands, which we define to be non-scaffold molecules that are capable of modulating the phase behavior of scaffolds via preferential binding (22). Phase separation sets up a phase boundary, which introduces a degree of freedom for ligand binding whereby the ligand can bind preferentially to the scaffold in one or the other phase. This preferential binding causes shifts in phase boundaries via linkage relations that can either enhance or weaken phase separation depending on whether the ligand binds preferentially to the scaffold in its dense versus dilute phase.

The *stickers*-and-*spacers* formalism (23-26, 36), which we model using coarse-grained simulations, allows us to uncover key features of ligands that destabilize or stabilize phase separation via preferential binding to scaffolds in the dilute versus dense phase, respectively. The features of ligands that contribute to their ability to modulate phase separation include the valence of scaffolding binding sites on ligands, the strengths of their interactions with scaffold sites, and the type of scaffold sites (stickers versus spacers) with which they interact. Given the interaction strength ranges studied here, our findings are as follows: Monovalent ligands weaken phase separation by either reducing the overall valence of the scaffold when they interact directly and favorably with sticker sites or by enhancing the effective excluded volume of spacers and weakening the cooperativity of the inter-sticker crosslinks that is needed for driving phase separation when they interact directly with spacer sites. Divalent ligands that bind to scaffold sites weaken phase separation when they compete directly with inter-sticker interactions that drive the phase separation of scaffolds. In contrast, divalent ligands that bind to spacer sites enable additional networking of multivalent scaffold molecules by serving as crosslinkers, thereby promoting phase separation. This finding is important in light of an ongoing debate about the relevance of phase separation *in vivo*, especially at endogeneous expression levels (43). Our results show that ligands can lower the saturation concentrations for scaffolds. Accordingly, scaffolds can

undergo ligand-mediated phase separation even if the endogeneous concentration of the scaffold is below its intrinsic saturation concentration – a feature that is likely amplified by the collective contributions of networks of ligands, providing they are multivalent (15, 16, 19).

The polyphasic linkage formalism provides a direct understanding of how ligand binding affects the dilute arms of phase boundaries when the dense arms are assumed to remain constant. Our simulations help us interrogate the effects of ligands on the concentrations of scaffolds within the dilute and the dense phase. The concentration of scaffolds within the dense phase stays similar to that of the unliganded case or decreases in the presence of ligand. This is true irrespective of whether or not the ligand binds preferentially to the scaffold in its dense or dilute phase. For preferential binding to the scaffold in the dense phase, c_A^L decreases, but the scaffold concentration in the dense phase (c_B^L) generally decreases when compared to c_B. This helps accommodate ligands that bind preferentially to scaffold sites in the dense phase. Conversely, for preferential binding to the scaffold in the dilute phase, c_A^L increases and c_B^L decreases compared to c_B. This dilution of scaffold within the dense phase derives from weakening the driving forces for phase separation.

Biomolecular condensates accommodate hundreds of distinct molecular components and considerable effort is being invested to understand the determinants of compositional control of distinct condensates (1, 9, 15, 17, 19, 34, 36, 44-50). Partition coefficients have become the workhorse quantities that are used to map the compositional biases of condensates (29, 34, 48, 51). Although, *PC*s are beneficial for compositional profiling of condensates, they do not yield insights as to whether the non-scaffold components of condensates act as modulators of scaffold phase behavior. This information is important if we want to be able to control condensate formation / dissolution.

We find that the *PC* can be greater than one irrespective of whether the ligand shows preferential binding to the scaffold in its dense or dilute phase or if the binding is agnostic across the phase boundary. This result derives from the fact that the *PC* is a convolution of the contributions from binding polynomials as well as the scaffold concentrations within the dense and dilute phases. Accordingly, a non-scaffold molecule can have a *PC* that is greater than one even if it destabilizes phase separation by binding preferentially to the scaffold in its dilute phase. This implies that if one is trying to find a molecular inhibitor of a condensate, knowing *PC*s for a set of molecules will not yield insights about which molecule would be the most effective inhibitor. Clearly, a *PC* that is less than one has significance, because it indicates that the molecule in question is being kept out of the condensate (50). However, this too will be due to a convolution of excluded volume effects and preferential interactions.

Our results suggest that the compositional profiling of condensates has to go beyond measuring partition coefficients to measuring saturation concentrations in order to understand what controls the precise formation / dissolution of condensates in the cell. For each non-scaffold constituent of a condensate, it is important to know if the molecule in question is a ligand that exhibits preferential binding to the scaffold across the phase boundary. If yes, does control over the expression level of the ligand provide cellular control over the stability of the condensate? To answer these questions, it is important to measure the effects of non-scaffold components on the phase boundaries of condensates. The simplest and most informative measurement would be a quantification of how c_A^L changes as a function of ligand concentration. Experimentally, this would

require tagging the scaffold molecule of interest in live cells and measuring its apparent threshold concentration (52) as the expression levels of ligands are tuned.

To this point, we have made the key assumption that a scaffold will be defined by a fixed saturation concentration. However, as noted in recent work (35, 53), this is only true if homotypic interactions among scaffold molecules are the primary drivers of phase separation. If condensates form via a combination of homotypic and heterotypic interactions (35, 53, 54), then the network of these interactions (12, 20) and hence a combination of scaffold concentrations will determine the location of the phase boundary and the slopes of tie lines. In this scenario, one would have to measure the effects of ligands on the location of the phase boundary, governed jointly by the concentrations of all scaffold molecules that drive phase separation. This would require measuring the concentrations of more than one scaffold molecule while titrating the concentration of the ligand in question. Further complexities will arise as we consider how networks of ligands impact the phase behavior of condensates that are governed by a network of homotypic and heterotypic interactions of scaffold molecules. These complexities are amenable to investigations using a combination of simulation, theory, and experiment that should provide a generalizable framework for designing cellular experiments and interpreting the results of these experiments.

Overall, our work suggests that one can exploit the fact that preferential binding requires an asymmetry of scaffold attributes across the phase boundary. Specifically, measuring the effect of small molecules (ideally, multivalent ligands) on c_A^L can be used as part of a chemical biology toolkit (55) to infer the features and internal organization of scaffolds within condensates. For example, if all molecules with a certain chemical structure / motif destabilize phase separation one can infer that the corresponding interaction motif in the scaffold is primarily accessible in the dilute phase and thus may be involved in driving phase separation. Such a strategy has the potential to lead to the rational design of therapeutics that modulate scaffold phase behavior in prescribed ways.

Materials and Methods

Full details of the LASSI simulations and corresponding analyses are given in the *SI Appendix*.

ACKNOWLEDGMENTS. This work was supported by grants from the US National Institutes of Health (5R01NS056114, 1R01NS089932) and Dewpoint Therapeutics Inc. (through a sponsored research agreement with Washington University in St. Louis). We thank Megan Cohan, Mina Farag, Alex Holehouse, Diana Mitrea, Mark Murcko, Michael Rosen, and Ammon Posey for helpful discussions.

References

1. S. F. Banani, H. O. Lee, A. A. Hyman, M. K. Rosen, Biomolecular condensates: organizers of cellular biochemistry. *Nature Reviews Molecular Cell Biology* **18**, 285-298 (2017).
2. Y. Shin, C. P. Brangwynne, Liquid phase condensation in cell physiology and disease. *Science* **357**, eaaf4382 (2017).
3. J. Berry, C. P. Brangwynne, M. Haataja, Physical principles of intracellular organization via active and passive phase transitions. *Reports on Progress in Physics* **81**, 046601 (2018).

4. J.-M. Choi, A. S. Holehouse, R. V. Pappu, Physical Principles Underlying the Complex Biology of Intracellular Phase Transitions. *Annual Review of Biophysics* **49**, 107-133 (2020).
5. A. A. Hyman, C. A. Weber, F. Jülicher, Liquid-liquid phase separation in biology. *Annu. Rev. Cell Dev. Biol.* **30**, 39-58 (2014).
6. O. Rog, S. Köhler, A. F. Dernburg, The synaptonemal complex has liquid crystalline properties and spatially regulates meiotic recombination factors. *eLife* **6**, e21455 (2017).
7. M. Kato *et al.*, Cell-free Formation of RNA Granules: Low Complexity Sequence Domains Form Dynamic Fibers within Hydrogels. *Cell* **149**, 753-767 (2012).
8. A. Patel *et al.*, A liquid-to-solid phase transition of the ALS protein FUS accelerated by disease mutation. *Cell* **162**, 1066-1077 (2015).
9. A. Molliex *et al.*, Phase separation by low complexity domains promotes stress granule assembly and drives pathological fibrillization. *Cell* **163**, 123-133 (2015).
10. C. P. Brangwynne, P. Tompa, R. V. Pappu, Polymer physics of intracellular phase transitions. *Nature Physics* **11**, 899-904 (2015).
11. X. Zeng, A. S. Holehouse, A. Chilkoti, T. Mittag, R. V. Pappu, Connecting Coil-to-Globule Transitions to Full Phase Diagrams for Intrinsically Disordered Proteins. *Biophysical Journal* **119**, 402-418 (2020).
12. P. Yang *et al.*, G3BP1 Is a Tunable Switch that Triggers Phase Separation to Assemble Stress Granules. *Cell* **181**, 325-345 e328 (2020).
13. C. J. Decker, R. Parker, P-Bodies and Stress Granules: Possible Roles in the Control of Translation and mRNA Degradation. *Cold Spring Harbor Perspectives in Biology* **4** (2012).
14. L. Stenström *et al.*, Mapping of the nucleolar proteome reveals spatiotemporal organization related to intrinsic protein disorder. *Molecular Systems Biology* **16**, e9469 (2020).
15. S. F. Banani *et al.*, Compositional Control of Phase-Separated Cellular Bodies. *Cell* **166**, 651-663 (2016).
16. P. Li *et al.*, Phase transitions in the assembly of multivalent signalling proteins. *Nature* **483**, 336-340 (2012).
17. T. P. Dao *et al.*, Ubiquitin Modulates Liquid-Liquid Phase Separation of UBQLN2 via Disruption of Multivalent Interactions. *Molecular Cell* **69**, 965-978.e966 (2018).
18. F. Fanalista, S. Deshpande, A. Lau, G. Pawlik, C. Dekker, FtsZ-Induced Shape Transformation of Coacervates. *Advanced Biosystems* **2**, 1800136 (2018).
19. X. Su *et al.*, Phase separation of signaling molecules promotes T cell receptor signal transduction. *Science* **352**, 595-599 (2016).
20. D. W. Sanders *et al.*, Competing Protein-RNA Interaction Networks Control Multiphase Intracellular Organization. *Cell* **181**, 306-324.e328 (2020).
21. J. Guillen-Boixet *et al.*, RNA-Induced Conformational Switching and Clustering of G3BP Drive Stress Granule Assembly by Condensation. *Cell* **181**, 346-361 e317 (2020).
22. J. Wyman, S. J. Gill, Ligand-linked phase changes in a biological system: applications to sickle cell hemoglobin. *Proceedings of the National Academy of Sciences* **77**, 5239 (1980).
23. M. Rubinstein, A. V. Dobrynin, Solutions of Associative Polymers. *Trends in Polymer Science* **5**, 181-186 (1997).
24. A. N. Semenov, M. Rubinstein, Thermoreversible Gelation in Solutions of Associative Polymers. 1. Statics. *Macromolecules* **31**, 1373-1385 (1998).

25. D. Deviri, S. A. Safran, Equilibrium size distribution and phase separation of multivalent, molecular assemblies in dilute solution. *Soft Matter* **16**, 5458-5469 (2020).
26. S. Ranganathan, E. I. Shakhnovich, Dynamic metastable long-living droplets formed by sticker-spacer proteins. *eLife* **9**, e56159 (2020).
27. T. P. Dao *et al.*, ALS-Linked Mutations Affect UBQLN2 Oligomerization and Phase Separation in a Position- and Amino Acid-Dependent Manner. *Structure* **27**, 937-951.e935 (2019).
28. Y. Yang, H. B. Jones, T. P. Dao, C. A. Castañeda, Single Amino Acid Substitutions in Stickers, but Not Spacers, Substantially Alter UBQLN2 Phase Transitions and Dense Phase Material Properties. *The Journal of Physical Chemistry B* **123**, 3618-3629 (2019).
29. J. Wang *et al.*, A Molecular Grammar Governing the Driving Forces for Phase Separation of Prion-like RNA Binding Proteins. *Cell* **174**, 688-699. e616 (2018).
30. S. Boeynaems *et al.*, Spontaneous driving forces give rise to protein−RNA condensates with coexisting phases and complex material properties. *Proceedings of the National Academy of Sciences USA* **116**, 7889-7898 (2019).
31. T. S. Harmon, A. S. Holehouse, M. K. Rosen, R. V. Pappu, Intrinsically disordered linkers determine the interplay between phase separation and gelation in multivalent proteins. *eLife* **6**, e30294 (2017).
32. T. S. Harmon, A. S. Holehouse, R. V. Pappu, Differential solvation of intrinsically disordered linkers drives the formation of spatially organized droplets in ternary systems of linear multivalent proteins. *New Journal of Physics* **20**, 045002 (2018).
33. A. E. Posey *et al.*, Profilin reduces aggregation and phase separation of huntingtin N-terminal fragments by preferentially binding to soluble monomers and oligomers. *Journal of Biological Chemistry* **293**, 3734-3746 (2018).
34. I. A. Klein *et al.*, Partitioning of cancer therapeutics in nuclear condensates. *Science* **368**, 1386 (2020).
35. J.-M. Choi, F. Dar, R. V. Pappu, LASSI: A lattice model for simulating phase transitions of multivalent proteins. *PLoS computational biology* **15** (2019).
36. J. R. Espinosa *et al.*, Liquid network connectivity regulates the stability and composition of biomolecular condensates with many components. *Proceedings of the National Academy of Sciences* **117**, 13238 (2020).
37. J. R. Simon, N. J. Carroll, M. Rubinstein, A. Chilkoti, G. P. Lopez, Programming molecular self-assembly of intrinsically disordered proteins containing sequences of low complexity. *Nature Chemistry* **9**, 509-515 (2017).
38. J. P. Brady *et al.*, Structural and hydrodynamic properties of an intrinsically disordered region of a germ cell-specific protein on phase separation. *Proc Natl Acad Sci U S A* **114**, E8194-E8203 (2017).
39. M. T. Wei *et al.*, Phase behaviour of disordered proteins underlying low density and high permeability of liquid organelles. *Nature Chemistry* **9**, 1118-1125 (2017).
40. E. W. Martin *et al.*, Valence and patterning of aromatic residues determine the phase behavior of prion-like domains. *Science* **367**, 694-699 (2020).
41. A. Ghosh, K. Mazarakos, H.-X. Zhou, Three archetypical classes of macromolecular regulators of protein liquid–liquid phase separation. *Proceedings of the National Academy of Sciences* **116**, 19474 (2019).

42. E. Freire, A. Schön, A. Velazquez-Campoy, "Chapter 5 Isothermal Titration Calorimetry: General Formalism Using Binding Polynomials" in Methods in Enzymology. (Academic Press, 2009), vol. 455, pp. 127-155.
43. D. T. McSwiggen, M. Mir, X. Darzacq, R. Tjian, Evaluating phase separation in live cells: diagnosis, caveats, and functional consequences. *Genes & Development* 10.1101/gad.331520.119 (2019).
44. Y. Lin, S. L. Currie, M. K. Rosen, Intrinsically disordered sequences enable modulation of protein phase separation through distributed tyrosine motifs. *Journal of Biological Chemistry* **292**, 19110-19120 (2017).
45. L. B. Case, X. Zhang, J. A. Ditlev, M. K. Rosen, Stoichiometry controls activity of phase-separated clusters of actin signaling proteins. *Science* **363**, 1093-1097 (2019).
46. T. H. Kim *et al.*, Phospho-dependent phase separation of FMRP and CAPRIN1 recapitulates regulation of translation and deadenylation. *Science* **365**, 825 (2019).
47. J. A. Greig *et al.*, Arginine-Enriched Mixed-Charge Domains Provide Cohesion for Nuclear Speckle Condensation. *Molecular Cell* **77**, 1237-1250.e1234 (2020).
48. J. A. Ditlev, L. B. Case, M. K. Rosen, Who's In and Who's Out—Compositional Control of Biomolecular Condensates. *Journal of molecular biology* **430**, 4666-4684 (2018).
49. W. Xing, D. Muhlrad, R. Parker, M. K. Rosen, A quantitative inventory of yeast P body proteins reveals principles of composition and specificity. *eLife* **9**, e56525 (2020).
50. M. C. Ferrolino, D. M. Mitrea, J. R. Michael, R. W. Kriwacki, Compositional adaptability in NPM1-SURF6 scaffolding networks enabled by dynamic switching of phase separation mechanisms. *Nature Communications* **9**, 5064 (2018).
51. S. Alberti, A. Gladfelter, T. Mittag, Considerations and Challenges in Studying Liquid-Liquid Phase Separation and Biomolecular Condensates. *Cell* **176**, 419-434 (2019).
52. Y. Shin *et al.*, Spatiotemporal Control of Intracellular Phase Transitions Using Light-Activated optoDroplets. *Cell* **168**, 159-171.e114 (2017).
53. J. A. Riback *et al.*, Composition-dependent thermodynamics of intracellular phase separation. *Nature* **581**, 209-214 (2020).
54. I. Alshareedah, M. M. Moosa, M. Raju, D. A. Potoyan, P. R. Banerjee, Phase transition of RNA−protein complexes into ordered hollow condensates. *Proceedings of the National Academy of Sciences* **117**, 15650 (2020).
55. M. J. C. Long, Y. Zhao, Y. Aye, Neighborhood watch: tools for defining locale-dependent subproteomes and their contextual signaling activities. *RSC Chemical Biology* **1**, 42-55 (2020).